

1 **OPTIMIZATION OF NANOPORES OBTAINED BY CHEMICAL ETCHING**
2 **ON SWIFT-ION IRRADIATED LITHIUM NIOBATE**

3
4 M. L. Crespillo^a, M. Otto^{a,1}, A. Munoz-Martin^a, J. Olivares^{b,a,*}, F. Agulló-López^{a,c},
5 M. Seibt^d, M. Toulemonde^e and C. Trautmann^f.

6
7 ^aCentro de Microanálisis de Materiales (CMAM), Universidad Autónoma de Madrid
8 (UAM), Cantoblanco, E-28049 Madrid, Spain.

9
10 ^bInstituto de Óptica, CSIC, C/Serrano 121, E-28006 Madrid, Spain.

11
12 ^cDepartamento de Física de Materiales, Universidad Autónoma de Madrid (UAM)
13 Cantoblanco, 28049 Madrid, Spain.

14
15 ^dIV.Physikalisches Institut. Universität Göttingen. Institut für Halbleiterphysik.
16 Tammannstr. 1. D-37077 Göttingen, Germany.

17
18 ^eCentre Interdisciplinaire de Recherche Ions-Lasers, UMR 11 CEA-CNRS, 14040
19 Caen Cedex, France.

20
21 ^fGesellschaft für Schwerionenforschung (GSI), Materialforschung, Planckstrasse 1,
22 64291 Darmstadt, Germany.

23
24
25 **Abstract**

26 The morphology of the nanopores obtained by chemical etching on ion-beam
27 irradiated LiNbO₃ has been investigated for a variety of ions (F, Br, Kr, Cu, Pb),
28 energies (up to 2300 MeV), and stopping powers (up to 35 keV/nm) in the electronic
29 energy loss regime. The role of etching time and etching agent on the pore morphology,
30 diameter, depth, and shape has also been studied. The transversal and depth profiles of
31 the pore have been found to be quite sensitive to both irradiation and etching
32 parameters. Moreover, two etching regimes with different morphologies and etching
33 rates have been identified.

36
37
38
39
40
41
42
43
44
45
46
47
48
49
50
51
52
53
54
55
56
57
58
59
60

*Corresponding author:

José Olivares, Instituto de Óptica, CSIC, C/Serrano 121, E-28006 Madrid, Spain.

E-mail: j.olivares@io.cfmac.csic.es, Tel.: +34 91 497 3670 Fax: +34 914973623

¹Presently at II. Physikalisches Institut. Universität Göttingen. Friedrich-Hund-Platz 1.
D-37077 Göttingen. Germany.

PACS: 81.07.-b; 61.80.Jh; 42.70.Mp.

Keywords: Nanopores, swift ion irradiation, ion tracks, AFM, lithium niobate.

1. Introduction

Nanometer-diameter amorphous tracks are generated by irradiation with swift ions on a variety of dielectric crystals and minerals whenever the electronic stopping power is above a certain threshold value¹⁻³ (i.e. 5 keV/nm for LiNbO₃). These tracks can be chemically etched to produce nanopores and a number of applications^{1,4,5} have been tested or suggested including fission-fragment dosimetry, molecular sieves, magnetic storage, field-emission displays,... For most applications the morphology of these nanopores has to be carefully controlled and optimized. So far, latent tracks in LiNbO₃ (LN), as relevant photonic material⁶, have been produced and characterized by RBS/C and optical methods^{7,8}. The kinetics of chemical etching has also been studied by⁹⁻¹² SEM and the etching rate measured by profilometry in experiments where the role of nuclear processes is significant⁹⁻¹². On the other hand, very scarce information is available¹³ on the detailed morphology of single etched tracks that is the relevant point for nano-patterning applications.

The purpose of this work is to extend and complement previous work¹³ to ascertain the role of irradiation conditions (ion energy, ion stopping power) and etching parameters on the morphology of etched tracks. Ions with input stopping powers from 3.4 keV/nm (F at 5 MeV) up to 35 keV/nm (Pb at 2300 MeV) have been used, so that the effects of electronic damage can be easily discriminated from those due to nuclear collisions. The role of thermal annealing after irradiation on the track morphology has been also investigated.

2. Experimental

Congruent LiNbO₃ (5x5 mm²) samples were cut from single crystal optical grade plates purchased from Photox Inc. They were irradiated at normal incidence in the

86 5 MV tandem accelerator installed at CMAM-UAM, in GANIL (Caen, France) and in
87 GSI (Darmstadt, Germany). The energies, stopping powers (at the surface) and
88 projected ranges of the ions used in this study are listed in Table I. Irradiation fluences
89 were in the $10^7 - 10^9 \text{ cm}^{-2}$ fluence range. Chemical etchings were performed at room
90 temperature (RT) in pure HF with concentrations of 5% and 40%, and blends of HF
91 (40%) with HNO₃ (70%) in 1:1 ratio. The main characterization technique used for the
92 examination of surface morphology was an AFM commercial instrument from Nanotec
93 Electrónica S.L. with phase-locked loop (PLL) feedback added to the dynamic or
94 tapping mode. Most measurements have been realized using commercial etched single-
95 crystalline silicon nitride tips with a nominal end radius of 10 nm and a resonant
96 frequency of 75 kHz. In certain cases high aspect ratio (>5:1) silicon tips (half cone
97 angle smaller than 5°) and radii of curvature less than 15 nm have been used. The
98 acquisition and analysis was made using the WSxM software, which is distributed
99 freely by Nanotec Electrónica S.L. AFM investigations were performed on X-cut
100 samples to avoid the strong tip-surface interaction typically observed through the
101 experience for Z-cut samples (piezoelectric behavior of LiNbO₃). For further structural
102 characterization of the nanopores the Philips CM200-FEG-UT transmission electron
103 microscope (TEM) was used. Samples were prepared with the focused ion beam (FIB)
104 and a gold film of 200 nm thickness was vapour deposited on the surface. All images
105 were recorded in bright field mode.

107 **3. Results**

108 *3.1. TEM data*

109 The TEM morphology of latent tracks generated on a LiNbO₃ sample (Z-cut) by
110 irradiation with Cu⁹⁺ ions at 51 MeV is illustrated in Fig. 1a captured with 40 kV.

111 The contrast is high enough to reveal the latent tracks. The tracks show a diameter value
112 of around 9 nm at the surface. For comparison the image of a crack of 18 nm diameter
113 and 305 nm depth is shown. The insets A and B in the figure correspond to the
114 diffraction patterns obtained on the crystalline region and inside the track respectively,
115 and they were recorded from a high resolution transmission electron microscope
116 (HRTEM) measurement with an acceleration voltage of 300 kV, similar to the one used
117 for the image shown in Fig. 1b. One notices the marked disorder apparent in the inset B.
118 In inset A, much more reflections are present than in B, which indicates that the crystal
119 structure changed and some kind of a phase transition has taken place. However we
120 have to take in account that since these HRTEM measurements are cross sections some
121 signal may come from the crystalline material surrounding the track. Further
122 investigations taking plan view measurements (i.e. along the track) must be carried out.

123 Fig. 1.b shows after etching time a very broad surface “crater” of 34 nm
124 diameter and 3.5 nm depth, whose symmetry axis is clearly shifted in relation to that for
125 the non-etched track.

126 127 3.2. *Effect of irradiation on nanopore morphology*

128 The track morphology after etching markedly depends on the irradiation conditions:
129 ion and energy. Some of the AFM pictures are shown in Fig. 2a, b, c and d,
130 corresponding to ions and energies indicated on the images. For stopping powers close
131 to the threshold value (5 keV/nm), as for F at 5 MeV (a), the shape of the nanopores
132 exhibits axial symmetry and is approximately circular. The same shape is also observed
133 for larger stopping powers at low enough etching times (≤ 10 min) and weaker acid
134 concentration (HF 5% and blends). On increasing stopping power and standard etching
135 times (20-60 minutes at RT) the pores clearly develop a pyramidal structure with well-

136 defined facets, as illustrated by the irradiations with Br at 46 MeV (Fig. 2b). At even
137 higher stopping powers, i.e. for irradiations with Kr at 800 MeV (Fig. 2c) and Pb at
138 2300 MeV (Fig. 2d), the faceting turns into a rather smooth and elongated profile. The
139 long axis lies at 33° from the z crystallographic axis (see Fig. 5.a) and so approximately
140 coincides with the easy cleavage plane⁶. Track etch pit has a double-shape well that was
141 also observed in our previous work¹³. It has been checked that the above morphological
142 trend is independent of the AFM tip used for the observations and the scanning
143 direction.

144 In order to better understand the origin of the pore asymmetry, we have investigated
145 the effect of Br irradiation at 46 MeV on +X and -X faces on the pore morphology. The
146 results are displayed in Fig. 3 that shows a chiral behavior i.e. the two pore images are
147 mirror images to each other.

148 3.3. *Effect of etching time in acid aqueous solutions.*

149 The evolution of the pore diameter and pore depth with etching time at RT is
150 respectively illustrated in Fig.4a and 4b for the irradiation with Br at 46 MeV. Data for
151 three acid solutions are included: HF at 40 %, HF at 5% and 1:1 mixture of both acids
152 (HF 40%, HNO₃ 70%). The most efficient etching is with HF at 40%. The etching rate
153 is much larger than that obtained in a previous study with a 1:1 mixture of HF and
154 HNO₃. The aspect ratio defined as depth/diameter is plotted in Fig. 4c.

155 3.4. *Influence of thermal annealing*

156
157 Thermal treatments after irradiation may anneal out some of the defects generated in
158 and around the track and thus influence the subsequent etching rates and pore
159 morphologies. The results are illustrated in Fig. 5 corresponding to the irradiation with
160

161 Br ions of 46 MeV, followed by, annealing in air for 60 minutes at various temperatures
162 as marked on the AFM images, and finally etched in HF 40%, for 60 minutes. One
163 observes that the annealing treatment does not remove entirely the latent tracks.
164 Moreover, it induces a clear elongation of the pore shape and gives rise to higher
165 surface aspect ratios.

167 **4. Conclusion**

168 Our extended set of etching experiments confirms that the pore morphology strongly
169 depends on the concentration of the acid solution and etching time. Pores initially
170 exhibit approximately axial symmetry but under extended etching they develop well
171 defined facets that correspond to particular crystalline planes. The faceted morphology,
172 not previously observed for LiNbO_3 , has also been observed in other crystals¹⁴.
173 Since LiNbO_3 is non centro symmetric, the morphology on the +X and -X faces of the
174 sample are mirror images from one another. Finally, many facets develop and the shape
175 rounds up but showing a very clear elongated anisotropy. The extrapolation of the data
176 in Fig. 4 to $t = 0$ indicate that the initial etching rate is quite fast up to about a (circular)
177 pore diameter of 10-40 nm and a depth of a few nanometers depending on the stopping
178 power of the ion. This fast stage could be associated to the track core (with a diameter
179 of a few nanometers) including the highly defective surrounding halo whose diameter
180 amounts to about 2-3 times that of the core¹⁵. The initial radial etch rate stage is
181 followed by a linear slower stage (where facets develop) that reaches an average
182 diameter of a few hundred of nanometers and a depth close to 100 nm. The slow stage
183 has a rate of a few nm/min depending on the concentration and composition of the acid
184 solution and should correspond to the etching of crystalline LiNbO_3 , i.e. the etching rate
185 should be essentially equal to that of the bulk unirradiated material.

186 **Acknowledgements:**

187 We acknowledge funding from the project MAT2005-06359-C03-02 from Ministry
188 of Education and Science of Spain. Authors acknowledge to the technical staff of
189 CMAM-UAM.

190
191
192
193
194
195
196
197
198
199
200
201
202
203
204
205
206
207
208
209
hal-00256612, version 1 - 30 Jul 2008

References

- [1] R. Spohr, in: K. Bethge (Ed.), *Ion tracks and Microtechnology, Basic Principles and Applications*, Vieweg, 1990.
- [2] G. Szenes, Phys. Rev. **B 51**, 8026 (1995).
- [3] A. Meftah, J.M. Costantini, N. Khalfaoui, S. Boudjadar, J.P. Stoquert, F. Studer and M. Toulemonde, Nucl. Instrum. Meth. Phys. Res. **B 237**, 563 (2005).
- [4] M. Toulemonde, C. Trautmann, E. Balanzat, K. Hjort and A. Weidinger, Nucl. Instrum. Meth. Phys. Res. **B 216**, 1 (2004).
- [5] J-H. Zollondz, and A. Weidinger, Nucl. Instrum. Meth. Phys. Res. **B 225**, 178 (2004).
- [6] R. S. Weis and T.K. Gaylord, *Applied Physics A: Materials Science and Processing*, **37**, 191 (2004).
- [7] S.M.M. Canut, R. Ramos, P. Brenier, J.L. Thevenard and M. Toulemonde, Nucl. Instrum. Meth. Phys. Res. **B 107**, 194 (1996).
- [8] J. Olivares, A. García-Navarro, G. García, A. Méndez and F. Agulló-López, Appl. Phys. Lett. **89**, 1 (2006).
- [9] M. Levy, R.M. Osgood Jr., R. Liu, E. Gross, G.S. Cargill III, A. Kumar, H. Bakhru, Appl. Phys. Lett. **73**, 2293 (1998).
- [10] C.L. Sones, S. Mailis, W.S. Brocklesby, R.W. Eason and J.R. Owen, J. Mater. Chem. **12**, 295 (2002).
- [11] J. Reinisch, F. Schrempel, T. Gischkat and W. Wesch, J. Electrochem. Soc. **155 (4)**, D298 (2008).
- [12] M. Bianconi, F. Bergamini, G.G. Bentini, A. Cerutti, M. Chiarini, P. De Nicola, G. Pennestri, Nucl. Instrum. Meth. Phys. Res. (2008) (in press).

- 234 [13] A. García-Navarro, A. Méndez, J. Olivares, G. García, F. Agulló-López, M. Zayat,
235 D. Levy and L. Vazquez, Nucl. Instrum. Meth. Phys. Res. **B 249**, 172 (2006).
- 236 [14] C. Trautmann, K. Schwartz, J. M. Costantini, T. Steckenreiter and M. Toulemonde,
237 Nucl. Instrum. Meth. Phys. Res. **107 B**, 367 (1998).
- 238 [15] J. Olivares, A. García-Navarro, G. García, A. Méndez and F. Agulló-López, Appl.
239 Phys. Lett. **89**, 071923 (2006).

240
241
242
243
244
245
246
247
248
249
250
251
252
253
254

255

6. Table list.

256

257

Table 1

258

Ion	Energy [MeV]	Energy [MeV/amu]	Se [keV/nm]	Rp [μm]
F	5	0.26	3.4	2.5
Br	12	0.15	6.1	3.2
Br	22	0.29	8.8	4.5
Br	46	0.57	12	6.7
Cu	51	0.80	12	7.2
Kr	800	10.4	13	60
Pb	2300	11.1	35	78

259

260

261

Table captions:

262

263

Table I: Energies, electronic stopping powers at the surface, (Se) and projected ranges (Rp) of the ions used.

264

265

266

267 **7. Figure captions.**

268
269 **Fig. 1.** TEM images of Cu 51 MeV irradiated LiNbO₃. (a) The light stripes indicate the
270 unetched tracks induced by ion bombardment; insets show the diffraction patterns;
271 (b) HRTEM image showing etched nanopore in cross sectional view.

272
273 **Fig. 2.** AFM images of different etch pit morphologies obtained after etching tracks
274 (HF 40% at RT for different times) produced with different kind of ions and energies:
275 (a) F 5 MeV, after 60 min., (b) Br 46 MeV, after 60 min., (c) Kr 800 MeV, after 10 min.
276 and (d) Pb 2300 MeV, after 10 min. Different AFM image sizes and depth-scales have
277 been used. The inset in (d) shows the depth profile recorded along the line across the
278 long axis of the two elongated pores. The lines are the polishing scratches revealed after
279 etching process in (a).

280
281 **Fig. 3.** AFM images of etched tracks on the + *X* face (a) vs. the -*X* face (b) of lithium
282 niobate after irradiation with Br 46 MeV and etched during 60 min in HF 40% at RT.
283 Revealed facets appear clearly in the excitation frequency image recorded by PLL mode
284 shown as inset in each case. Depth-scale: 30 nm.

285
286 **Fig. 4.** Pore dimensions versus etching time for different etching solutions using
287 samples irradiated with Br ions of 46 MeV. (a) Long axis diameter, (b) pore depth, and
288 (c) aspect ratio (depth/ short axis diameter).

289
290 **Fig. 5.** AFM images of pore morphologies obtained for samples irradiated with Br
291 ions of 46 MeV and subjected to annealing in air for 1 hour at different temperatures,
292 prior to the etching process (HF 40%, 1 hour at RT). Depth-scale: 30 nm.

8. Figures

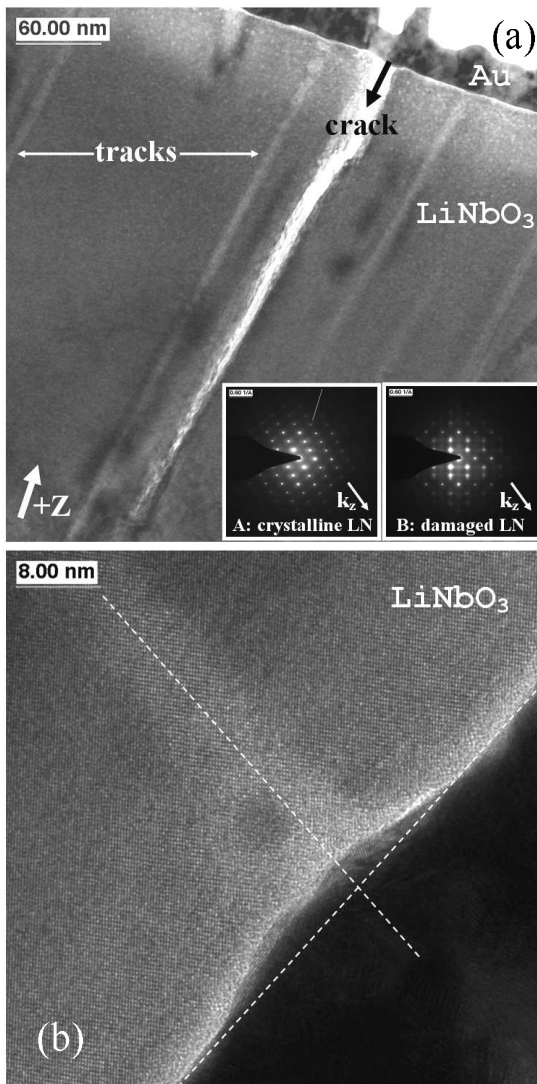


Fig. 1

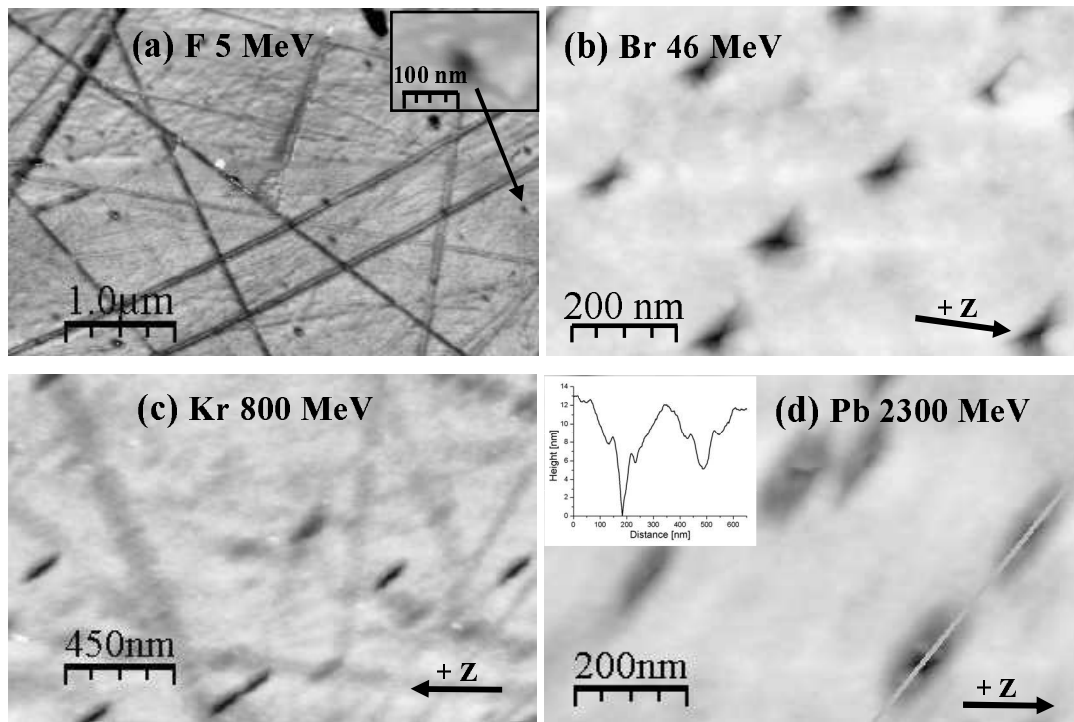


Fig. 2

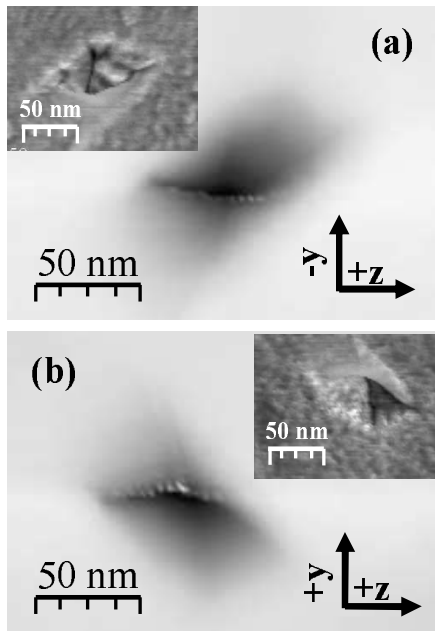


Fig. 3

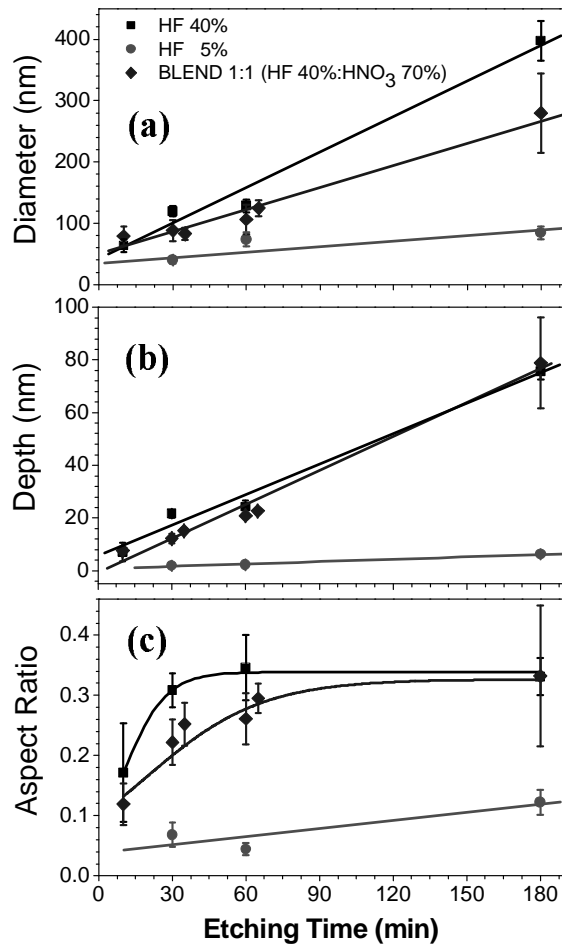


Fig. 4

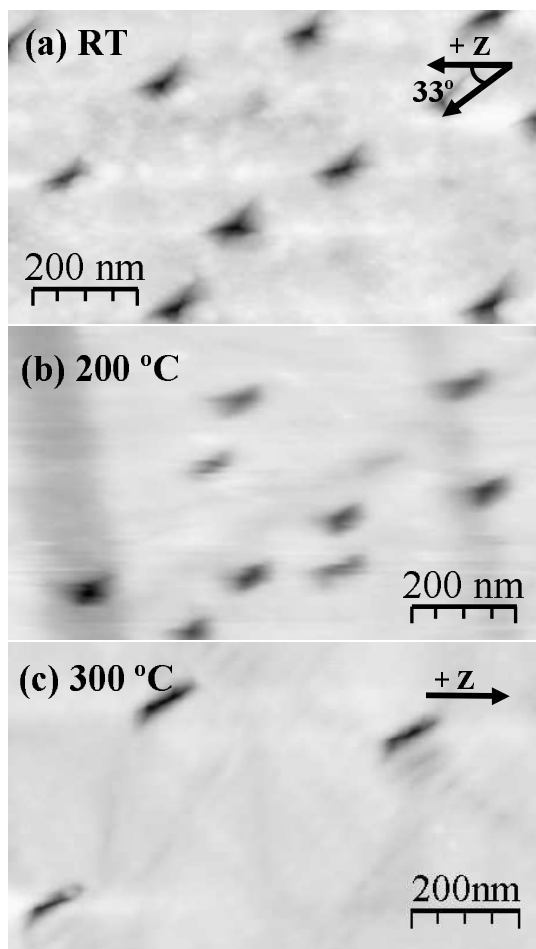


Fig. 5